Available online at www.sciencedirect.com
SCIENCE DIRECT®
International Journal of Heat and Mass Transfer 47 (2004) 1847–1862
International Journal of HEAT and MASS TRANSFER
www.elsevier.com/locate/ijhmt

Structure of vertical downward bubbly flow

Takashi Hibiki [a], Hiroshi Goda [b], Seungjin Kim [b], Mamoru Ishii [b,*], Jennifer Uhle [c]

[a] Research Reactor Institute, Kyoto University, Kumatori, Sennan, Osaka 590-0494, Japan
[b] School of Nuclear Engineering, Purdue University, 400 Central Drive, West Lafayette, IN 47907-2017, USA
[c] Division of System Analysis and Regulatory Effectiveness Office of Research, US Nuclear Regulatory Commission, Washington, DC 20555, USA

Received 30 September 2003; received in revised form 9 October 2003

Abstract

In view of the great importance to two-fluid model, structure of downward bubbly flows in vertical pipes has been discussed intensively based on available data sets of local flow parameters including extensive air–water data sets recently measured by the authors. In this study, an approximate radial phase distribution pattern map has been proposed based on available data sets, and radial profiles of local flow parameters such as void fraction, interfacial area concentration, interfacial velocity, and bubble Sauter mean diameter have been discussed in detail. The one-dimensional drift-flux model for a downward two-phase flow and the correlation of the interfacial area concentration have been compared with the downward flow data. The correlations applicable to the predictions of one-dimensional void fraction and interfacial area concentration for a downward bubbly flow have been recommended by the comparison.

Keywords: Void fraction; Interfacial area concentration; Bubble size; Drift-flux model; Gas–liquid bubbly flow; Downward flow; Multiphase flow

1. Introduction

The void fraction and interfacial area concentration are two fundamental geometrical parameters in a bubbly two-phase flow. The void fraction expresses the phase distribution and is a required parameter for hydrodynamic and thermal design in various industrial processes. On the other hand, the interfacial area describes available area for the interfacial transfer of mass, momentum and energy, and is a required parameter for a two-fluid model formulation. Various transfer mechanisms between phases depend on the two-phase interfacial structures. Therefore, an accurate knowledge of these parameters is necessary for any two-phase flow analyses. This fact can further be substantiated with respect to two-phase flow formulation.

In view of the great importance to two-fluid model, local measurements of these flow parameters such as void fraction and interfacial area concentration have been performed in a bubbly flow intensively over the past 10 years [1–5]. However, most of the experiments were performed for upward two-phase flows in vertical pipes, and quite little attention has been paid to local flow measurements in downward two-phase flows. Some flow measurements of local flow parameters such as phase distribution and turbulent structure have been performed in downward two-phase flows with liquid velocity lower than 1 m/s [6–8]. The flow structures such as void "coring" have been clarified partially by these studies. However, no measurement was performed for local interfacial area concentration and gas velocity in a downward two-phase flow.

* Corresponding author. Tel.: +1-765-494-4587; fax: +1-765-494-9570.
E-mail addresses: hibiki@rri.kyoto-u.ac.jp (T. Hibiki), ishii@ecn.purdue.edu (M. Ishii).

0017-9310/$ - see front matter © 2003 Elsevier Ltd. All rights reserved.
doi:10.1016/j.ijheatmasstransfer.2003.10.027

Nomenclature

A	lift parameter
a_i	interfacial area concentration
$\tilde{a}_i$	non-dimensional interfacial area concentration
C_0	distribution parameter
C_{w1}	coefficient
C_{w2}	coefficient
D	pipe diameter
D_b	bubble diameter
$D_{b,2}$	diameter of group-II bubble
$D_{b,2,max}$	maximum bubble diameter
$D^*_{b,2}$	non-dimensional diameter of group-II bubble
$D_{d,max}$	maximum distorted bubble limit
D_{Sm}	Sauter mean diameter
$\widetilde{D}_{Sm}$	non-dimensional Sauter mean diameter
g	gravitational acceleration
j	mixture volumetric flux
j^*	non-dimensional mixture volumetric flux
j_C	mixture volumetric flux at channel center
j_g	superficial gas velocity
j_f	superficial liquid velocity
K_B	constant
K_C	constant
L	pipe length
Lo	Laplace length
$\widetilde{Lo}$	non-dimensional Laplace length
M_f	lift force
M_w	wall repulsion force
m	exponent
N	bubble number
n	exponent
P	pressure
R	pipe radius
R_b	bubble radius
$\widetilde{Re}$	Reynolds number
R_P	radial position where void fraction becomes zero
r	radial coordinate
V_{gj}	void fraction-weighted mean drift velocity
V_r	relative velocity of vortex centers with edge of viscous sublayer
v_g	interfacial velocity or gas velocity
v^*_g	non-dimensional gas velocity
v_f	liquid velocity
v_r	relative velocity
We	Weber number
y_0	distance from wall to bubble center
z	axial coordinate

Greek symbols

α	void fraction
α_C	void fraction at channel center
Γ_B	constant
Γ_C	constant
$\Delta\rho$	density difference
δ_b	average distance of void peak from wall
δ_v	viscous sublayer thickness
ε	energy dissipation rate per unit mass
ν_f	kinematic viscosity
ρ_g	gas density
ρ_f	liquid density
ρ_m	mixture density
σ	interfacial tension
Φ_f	square of two-phase frictional multiplier based on pressure gradient of liquid flow
Ω	centrifugal force per unit mass
ω	group-II bubble classification rate

Subscripts

A	quantity after correction
B	quantity before correction
calc.	calculated value
meas.	measured value
1	group-I bubble
2	group-II bubble

Mathematical symbols

$\langle\ \rangle$	area-averaged quantity
$\langle\langle\ \rangle\rangle$	void fraction weighted cross-sectional area-averaged quantity

From this point of view, the authors recently measured local flow parameters of downward air–water bubbly flows such as void fraction, interfacial area concentration, gas velocity, and bubble diameter in vertical pipes with inner diameters of 25.4 and 50.8 mm [9]. Based on the local flow measurements of vertical downward bubbly flows, this study aims at (1) extensive review of the existing local flow data, (2) interpretation of the measurement results, (3) intensive discussion of local flow characteristics and (4) evaluation of existing drift-flux correlation and interfacial area concentration correlation by the data, and recommendation of the correlations applicable to the prediction of one-dimensional void fraction and interfacial area concentration for a downward bubbly flow.

2. Databases

Recently, the authors measured local flow parameters of downward air–water bubbly flows such as void fraction, interfacial area concentration, and gas velocity in

vertical pipes with inner diameters of 25.4 and 50.8 mm by means of a multi-sensor conductivity probe [9]. In what follows, the apparatus and the results are briefly explained.

Fig. 1 shows the schematic diagram of the two-phase flow loop. The test loop consisted of two test sections, which were 25.4 and 50.8 mm inner diameter acrylic pipes, whose total lengths, L, non-dimensionalized by the pipe diameter, D, were $L/D = 150$ and 75, respectively. The test loop was designed for upward and downward two-phase flow experiments. Air was supplied by a compressor, and was introduced into a mixing chamber through the two-phase injection unit. The two-phase injection unit was composed of a gas injection

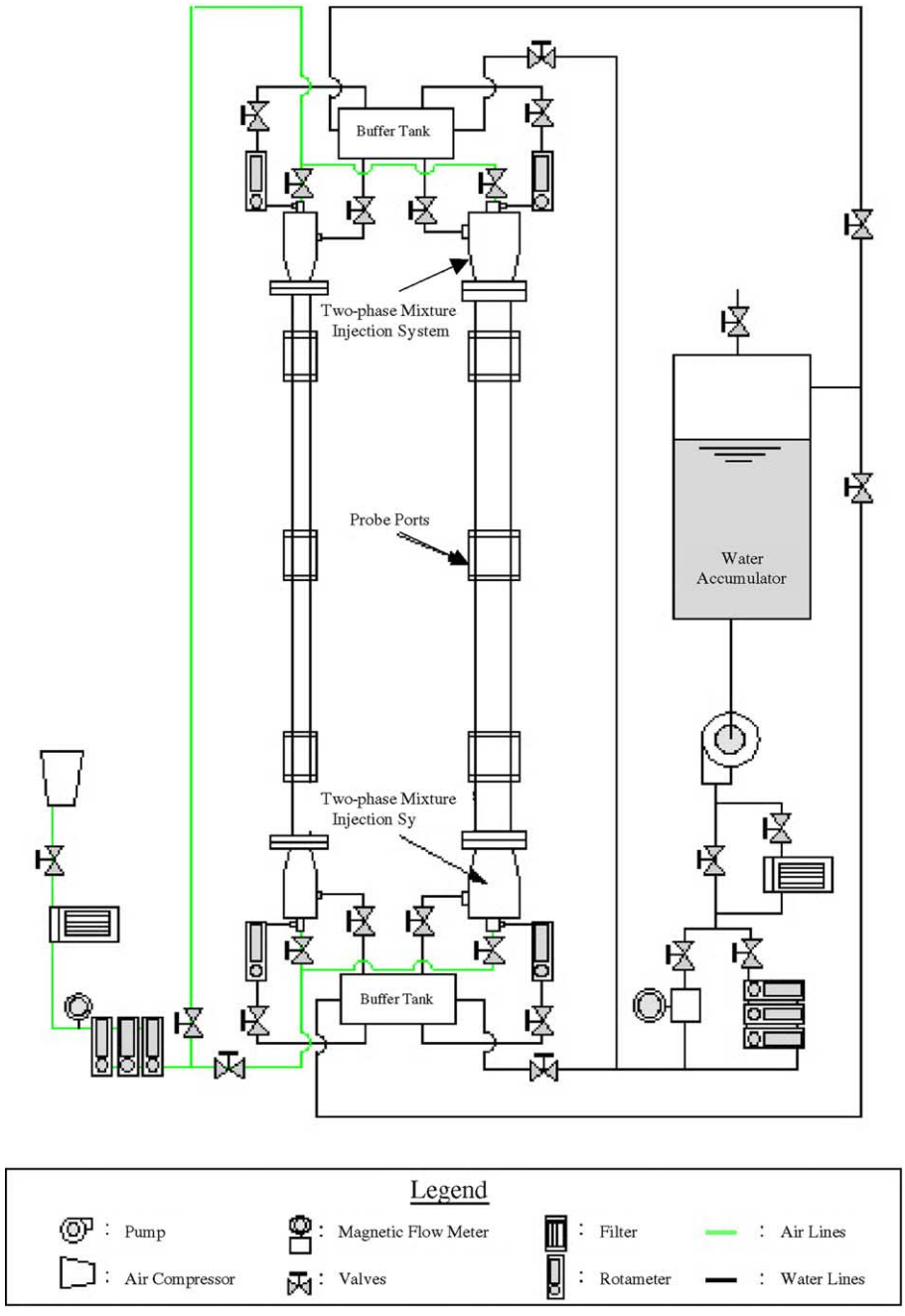

Fig. 1. Schematic diagram of the experimental loop [9].

section and a liquid injection section. A sparger unit was employed as a bubble generator for the gas injection section. The porous material with 10 μm pores was used for the sparger units, which produced uniform bubbles of approximately 1–2 mm in size. The liquid injection section was composed of two separate parts: primary liquid injection line for controlling total liquid flow rate, and secondary liquid injection line for controlling the inlet bubble size. The flow rate in the secondary liquid injection line, which controlled the inlet bubble size, was kept constant at the gas superficial velocity of 0.09 m/s throughout the experiment in order to keep the inlet bubble size constant. The total liquid flow rate was achieved by varying the flow rate in the primary liquid injection line. The primary liquid injection line was further separated into three equally spaced inlets with 120°. This was in order to prevent the formation of vortices, and also to provide a uniform supply of liquid in the injection unit. Immediately preceding the injection unit, a buffer tank was utilized in order to deliver liquid uniformly to the primary and secondary liquid injection lines. The air and purified water were mixed in the mixing chamber, and the mixture flowed downward through the test section. The flow rates of the air and water were measured with a rotameter and a magnetic flow meter, respectively. The local flow parameters such as void fraction, interfacial area concentration, interfacial velocity, and bubble Sauter mean diameter were measured by using a multi-sensor conductivity probe, which has been validated in the previous work [10]. The measurement accuracies of void fraction, interfacial area concentration and gas velocity were benchmarked by other calibration instrumentations such as a gamma densitometer, a photograph, and a rotameter, respectively, and were estimated to be within ±5.74%, ±6.95%, and ±12.4%, respectively [4,5]. The multi-sensor conductivity probe methodology is detailed in the paper [10].

The local measurements were performed at $z/D = 66.5$ and 133 for 25.4- and 50.8-mm pipes, respectively, where z is the axial location measured from the test section inlet. In the local measurements of flow parameters such as interfacial area concentration and gas velocity, the superficial liquid velocity, $\langle j_f \rangle$, and the void fraction, $\langle \alpha \rangle$, ranged from −1.25 to −3.11 m/s and from 1.40% to 19.1%, respectively, for $D = 25.4$ mm, and from −0.620 to −2.49 m/s and from 0.211% to 6.94%, respectively, for $D = 50.8$ mm [9]. Here, $\langle\ \rangle$ means the area-averaged quantity, and the negative sign of the superficial liquid velocity indicates the downward direction. On the other hand, local void fraction measurements were performed in the ranges of $1.40\% \leqslant \langle \alpha \rangle \leqslant 65.7\%$ for $D = 25.4$ mm and $0.211\% \leqslant \langle \alpha \rangle \leqslant 76.9\%$ for $D = 50.8$ mm by means of a single front-sensor among four sensors in the multi-sensor probe. The detailed flow conditions are tabulated in Table 1. The local void fraction distributions obtained in the experiment agree with those observed by various investigators [6–8]. This indicates that the new data obtained in the experiment would be considered to be reasonable as a database.

In addition to this database, following three databases [6–8] are available. Wang et al. [6] studied turbulence structure and phase distribution of downward bubbly flows in a vertical pipe with an inner diameter of 57.2 mm. They measured local flow parameters such as void fraction, liquid velocity, and Reynolds stress at $z/D = 35$. In their experiment, the area-averaged superficial liquid velocity and the void fraction ranged from −0.43 to −0.94 m/s and 6.83% to 32.4%, respec-

Table 1
Flow conditions in the data base

$\langle j_f \rangle$ (m/s)	D (mm)	z/D (–)	$\langle j_{g,N} \rangle$ (m/s)		
			Symbols: ●	▲	■
−1.25	25.4	133	−0.0177 (1.40)[a] transition	−0.0993 (6.71)[a] bell	−0.289 (19.1)[a] bell
−2.12	25.4	133	−0.102 (3.24)[a] bell	−0.381 (15.5)[a] bell	N/A
−3.11	25.4	133	−0.106 (2.87)[a] bell	−0.487 (11.8)[a] core	N/A
−0.620	50.8	66.5	−0.00427 (0.420)[a] off-center	−0.0466 (6.22)[a] bell	N/A
−1.25	50.8	66.5	−0.00427 (0.211)[a] off-center	−0.0272 (1.63)[a] transition	−0.0882 (5.92)[a] transition
−2.49	50.8	66.5	−0.0307 (0.694)[a] transition	−0.0976 (2.43)[a] transition	−0.189 (5.20)[a] transition
			Symbols: ○	△	□
0.872	25.4	125	0.0414 (5.09)[a]	0.0813 (9.35)[a]	0.143 (15.2)[a]
1.75	25.4	125	0.0461 (3.14)[a]	0.116 (7.31)[a]	0.257 (14.4)[a]
3.49	25.4	125	0.0509 (1.83)[a]	0.201 (6.57)[a]	0.516 (15.1)[a]
0.491	50.8	53.5	0.0275 (4.90)[a]	0.0556 (9.20)[a]	0.129 (19.2)[a]
0.986	50.8	53.5	0.0473 (5.12)[a]	0.113 (10.8)[a]	0.242 (20.3)[a]
2.01	50.8	53.5	0.103 (5.68)[a]	0.226 (10.8)[a]	0.471 (18.3)[a]

N/A = Not available.

[a] Values in the parentheses mean the void fractions in %.

tively. Usui and Sato [7] studied phase distribution of downward two-phase flows in vertical pipes with inner diameters of 16 and 24 mm. They measured local void fractions at $z/D = 100$. In their experiment, the area-averaged superficial liquid velocity and the void fraction ranged from −0.332 to −1.0 m/s and 6.43% to 88.3%, respectively. Kashinsky and Randin [8] studied turbulence structure and phase distribution of downward bubbly flows in a vertical pipe with an inner diameter of 42.3 mm. They measured local flow parameters such as void fraction, liquid velocity, and turbulence intensity. In their experiment, the area-averaged superficial liquid velocity and the void fraction ranged from −0.50 to −1.0 m/s and 2.21% to 17.0%, respectively. These databases will be utilized to discuss the structure of a vertical downward two-phase flow.

3. Results and discussion

3.1. Local flow parameters

3.1.1. Phase distribution pattern

Fig. 2 shows void fraction profiles of downward bubbly flows measured in vertical pipes with $D = 25.4$ mm (upper figure) and 50.8 mm (lower figure). For comparison, void fraction profiles of upward bubbly flows measured in vertical pipes with $D = 25.4$ mm (upper figure) [4] and 50.8 mm (lower figure) [5] are also shown in Fig. 3. The meanings of the symbols in Figs. 2 and 3 are found in Table 1.

Recently, Hibiki et al. [11] classified the phase distribution pattern of upward bubbly flows into three basic types, that is, (i) wall-peaked, (ii) core-peaked, and (iii) flat distributions. However, as shown in Figs. 2 and 3, the phase distribution patterns observed in downward bubbly flows are quite different from those in upward bubbly flows. The phase distribution patterns observed in downward flows may roughly be classified into three basic types, that is, (i) off-center-peaked, (ii) bell-typed, and (iii) core-peaked distributions. The off-center-peaked distribution is characterized by an off-center peak, which is not sharper than wall peak often observed in upward bubbly flows. The bell-typed distribution is characterized by a core peak with an inflection point and a skirt near the wall. The core-peaked distribution is characterized by a peak at the channel center, namely a typical power-law profile.

The classified results for the phase distributions shown in Fig. 2 are given in Table 1. Fig. 4 shows an approximate map of phase distribution patterns based on downward flow experiments performed by different

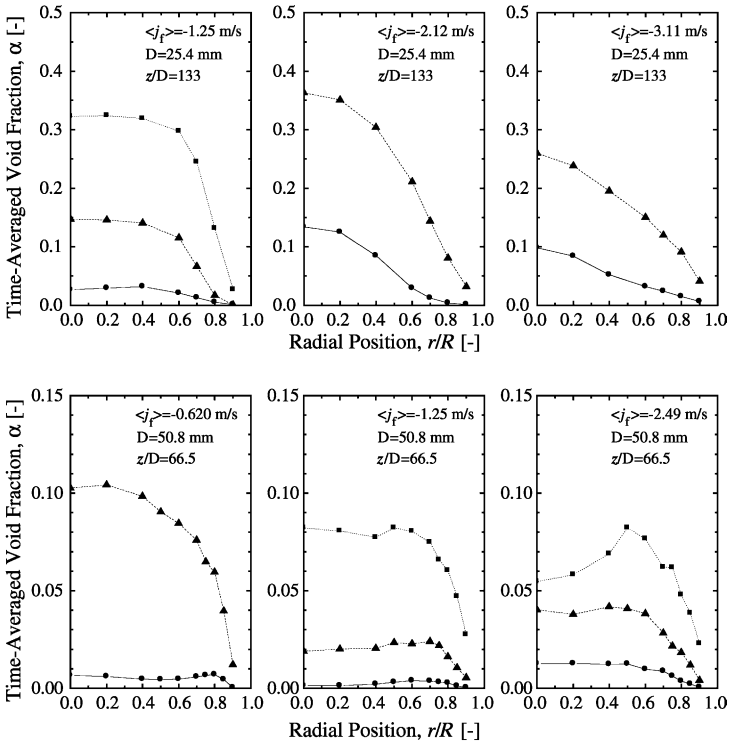

Fig. 2. Local void fraction profiles of downward bubbly flows measured in vertical pipes with $D = 25.4$ mm (upper figure) and 50.8 mm (lower figure).

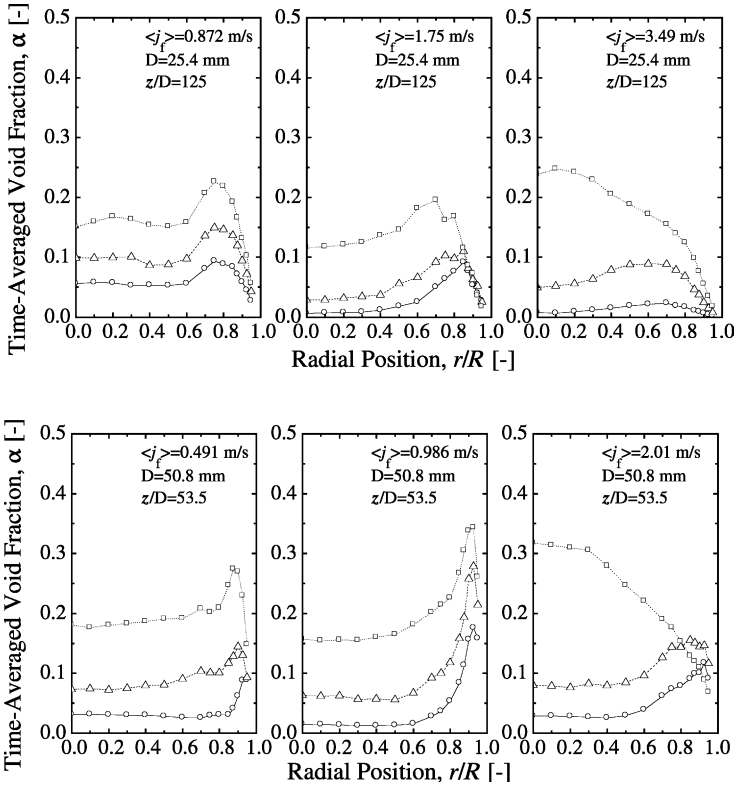

Fig. 3. Local void fraction profiles of upward bubbly flows measured in vertical pipes with $D = 25.4$ mm (upper figure) and 50.8 mm (lower figure).

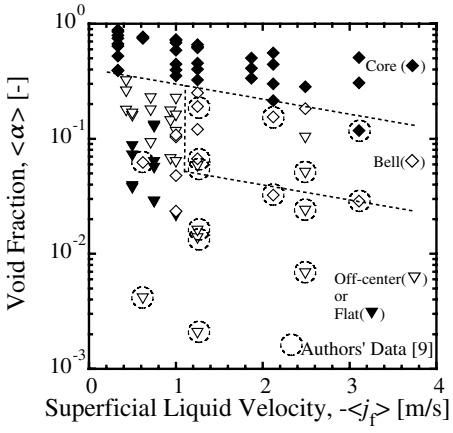

Fig. 4. Map of phase distribution patterns (original void distribution data are cited from [6–9]).

scientists [6–9] with different types of bubble injections in vertical pipes (16 mm $\leqslant D \leqslant$ 57.2 mm). The classification shown in Fig. 4 is performed by the present authors. The detailed flow conditions are explained in the section of "database". The open reversed triangles, open diamonds, and solid diamonds indicate the off-center-peaked, bell-typed, and core-peaked distributions. In addition to these, flat distributions, which are characterized by flat distribution along the channel radius ($r/R \leqslant 0.8$) with a relatively steep decrease near the wall ($r/R \geqslant 0.8$), are indicated by solid reversed triangles. The flat distribution may be considered the transition between the off-centered and bell-typed distributions. It should be noted here that broken lines in Fig. 4 indicate only rough phase distribution boundaries drawn by the limited database, and the dotted circles in Fig. 4 indicates the present data [9]. Since some data do not exist in the region bounded by the phase distribution boundaries, the boundary lines proposed as the first attempt are to be modified by more data to be taken in a future study.

For relatively higher void fractions, core-peaked void distributions are observed. The phase distribution pattern transition boundary between the core-peaked and bell-typed distributions is likely to be dependent on the superficial liquid velocity. The increase in the liquid velocity tends to decrease the void fraction at the phase distribution pattern transition. For medium void fractions and superficial liquid velocities higher than 1.0 m/s, bell-typed void distributions are observed, whereas for low void fractions and low superficial liquid velocities,

off-center-peaked void distributions are observed. The early work on the phase distribution in a downward bubbly flow showed that the radial void distribution peaked at the center of the channel [6,12]. However, some local maxima in the void fraction distribution close to the wall has been reported by Kashinsky and Randin [8] at low liquid velocity ($\langle j_f \rangle = 0.50$ m/s) and relatively high void fraction and by Ganchev and Peresadko [13] at low liquid velocity. In addition to these flow conditions, this study reveals that the off-center-peaked void fraction distributions also exist in the region of relatively low void fraction ($\langle \alpha \rangle \leqslant 5\%$) and high liquid velocity ($\langle j_f \rangle \geqslant 1$ m/s).

Wang et al. [6] explained the "coring" void phenomena by the interfacial lift force. For a fully developed axisymmetric pipe flow, the lift force, M_f is given by

$$M_f = A\rho_f \alpha v_r \frac{\partial v_f}{\partial r}, \tag{1}$$

where A, ρ_f, v_r and v_f are the lift parameter, the liquid density, the relative velocity, and the liquid velocity, respectively. Wang et al. [6] developed an empirical correlation of the lift parameter based on their experimental data, and predicted their "coring" void distributions by the radial momentum equation and the lift force satisfactorily. The empirical correlation of the lift parameter ($A > 0$) indicated that the lift force in the tested downward flows always pushed the bubbles toward the channel center. They demonstrated that the turbulence-induced lateral pressure field and the lateral lift forces determined how the voids distributed radially. It should be noted here that the bubble migration characteristics in an upward flow are quite different from those in a downward flow. It is well-known experimentally [1,14] that the direction of the bubble migration in an upward bubbly flow is dependent on the bubble size. Tomiyama et al. [15] experimentally classified the bubble lateral migration regime in a vertical upward bubbly flow into three regimes, namely (i) wall regime: $0.4 < D_b < 5$ mm, (ii) neutral regime: $0 < D_b < 0.4$ mm, $5 < D_b < 6$ mm, and (iii) core regime: 6 mm $< D_b$, where D_b is the bubble diameter. The experimentally determined lift parameter in wall or core regime is significant positive or negative value, respectively, whereas the experimentally determined lift parameter in neutral regime is very small. Thus, the significant lift force toward the channel wall or center acts on the bubbles in wall or core regime, respectively. On the other hand, since the lift force in neutral regime might be insignificant, Tomiyama et al. [15] suggested that the bubble lateral migration in an upward bubbly flow might be affected by many other factors such as liquid turbulence.

Lately, Kashinsky and Randin [8] also attempted to explain the "coring" void phenomena by the interfacial lift and wall repulsion forces. The wall repulsion force, M_w, is given by [16]

$$M_w = -\frac{\alpha\rho_f v_r^2}{R_b^2}\left\{C_{w1} + C_{w2}\left(\frac{R_b}{y_0}\right)\right\}, \tag{2}$$

where R_b, C_{w1}, C_{w2}, and y_0 are the bubble radius, a coefficient given by $-0.06v_r - 0.104$, a coefficient to be 0.147, and the distance from the wall to the bubble center, respectively. It should be noted here that this force has the same sign between upward and downward flows. The wall repulsion force always pushes the bubbles from the wall. Kashinsky and Randin [8] suggested that since both of lift and wall repulsion forces in a downward flow would push the bubble away from the wall, a bubble-free region near the wall, which was defined as a bell-typed or flat void distribution in this study, could be created. Thus, the bell-typed and core-peaked void distributions can be explained by the forces acting on the bubbles, whereas the lift and wall repulsion forces may not be enough to explain the off-center-peaked void distribution.

Usui and Sato [7] pointed out that there seemed to be another factor governing the void distribution in addition to the lift force due to the velocity profile. The bubble shape deformed by the turbulence and velocity gradient in the liquid phase might change the velocity field surrounding bubbles with a change in the pressure field. Usui and Sato [7] inferred that the change might make bubbles be apt to migrate toward the wall, making an attempt to avoid the fast moving liquid in the central part of the pipe.

The wall-vortex effect model proposed by Rohani [17] may explain the off-center-peaked void distribution in a downward bubbly flow. According to his model, the centrifugal force per unit mass, Ω, due to rolling vortices sliding along the viscous sublayer near the wall is given by

$$\Omega = \frac{V_r^2}{\delta_b - \delta_v}, \tag{3}$$

where V_r, δ_b and δ_v are the relative velocity of the vortex centers with the edge of the viscous sublayer, the average distance of the void peak from the wall, and the viscous sublayer thickness, respectively. Such a centrifugal force due to rolling vortices always pushes the bubbles toward the wall, resulting in an off-center-peaked void fraction distribution even in a downward bubbly flow.

Unfortunately, in spite of much efforts described above, a widely accepted model has not been obtained to explain the off-center-peaked void fraction distribution so far. In this section, only possible mechanisms are introduced. Since the present data bases are not sufficient to conclude the mechanism of the off-center peak void fraction profile in a downward two-phase flow, further theoretical and experimental studies should be

encouraged to explain the mechanism of the bubble migration in a downward two-phase flow.

3.1.2. Void fraction

To discuss the bubble migration and coalescence characteristics, spherical and distorted bubbles are categorized as group I, and the cap and Taylor bubbles are categorized as group II. In identifying the bubble types, the maximum distorted bubble limit, $D_{d,max}$, is used as a criterion [18], such that

$$D_{d,max} = 4\sqrt{\frac{\sigma}{g\Delta\rho}}, \tag{4}$$

where σ, g, and $\Delta\rho$ are the surface tension, the gravitational acceleration, and the density difference, respectively. For an air–water flow at atmospheric pressure and 20 °C, the maximum distorted bubble size is estimated to be 10.9 mm. The bubble types are approximately classified by measured chord length and the criterion given by Eq. (4), see Appendix A.

Fig. 5 shows the ratio of void fraction of cap bubbles, $\langle\alpha_2\rangle$, to total void fraction, $\langle\alpha\rangle$ as a parameter of the superficial liquid velocity. It was reported that the cap bubble formation started at $\langle\alpha\rangle \approx 15\%$ for an upward bubbly flow [4,5], whereas it starts at the void fraction much smaller than 15% for a downward bubbly flow. The cap bubble formation in a downward flow at smaller $\langle\alpha\rangle$ may be attributed to the bubble migration characteristics in a downward flow, which are quite different from those in an upward flow.

As explained in the previous section, the bubbles in a downward flow more or less tend to migrate toward the channel center regardless of the bubble size, whereas the direction of the bubble migration in an upward flow strongly depends on the bubble size. Forces acting on bubbles in a downward flow more or less tend to localize bubbles around the channel center, which means that bubble populations near the channel center and wall are extremely high and low, respectively. Thus, the bubble migration toward the channel center in the downward flow increases the bubble population near the channel center, which enhances the probability of bubble collision resulting in the bubble coalescence. Since large bubbles formed by coalescence can stay around the channel center due to the force acting on the large bubbles, successive coalescence between the large bubbles or coalescence between the large bubbles and the bubbles migrated from the channel wall may occur around the channel center resulting in the formation of cap bubbles easily.

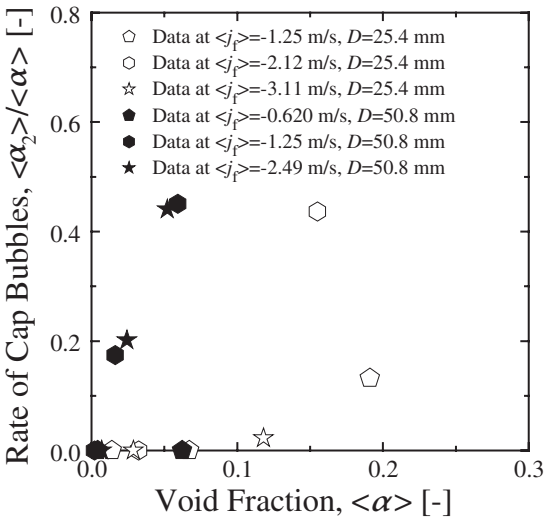

Fig. 5. Ratio of void fraction of cap bubbles to total void fraction.

To discuss the cap bubble formation process in an upward flow, we consider the bubbles distributed uniformly with the diameter of about 3 mm at the channel inlet corresponding to the bubbly flows shown in Fig. 3 [4,5]. In such a bubbly flow, bubbles with relatively small diameter ($0.4 < D_b < 5$ mm; wall regime) tend to migrate toward the channel wall where the population of bubbles with relatively small diameter is extremely high. Thus, the bubble collision between the relatively small bubbles would be enhanced near the channel wall. When the size of the coalesced bubbles exceeds 6 mm, the direction of the lift force acting on the bubbles is reversed and they start moving toward the channel center. This may hinder the successive coalescence between the large bubbles near the channel wall, and thus cap bubbles may not easily be formed near the channel wall. Since relatively large bubbles formed in the vicinity of the channel wall are migrated toward the channel center, the void fraction around the channel center gradually increases along the flow direction and eventually cap bubbles may be formed around the channel center. Thus, when the formation of cap bubbles starts in an upward flow, local void fraction would be high around not only the channel wall but also the channel center, resulting in relatively high average void fraction. On the other hand, local void fraction near the channel wall is extremely low at the initiation of the formation of cap bubbles in a downward flow, resulting in relatively low average void fraction. This may be the reason why the average void fraction in a downward flow is smaller than that in an upward flow at the initiation of the cap bubble formation.

Fig. 5 shows that a larger diameter pipe tends to form cap bubbles easily. This may be explained by the liquid turbulence. Recently, Hibiki and Ishii [19] derived a transition criterion of dominant phenomena for bubble coalescence and breakup from the interfacial area transport equation as

$$\langle\alpha\rangle = \frac{(\Gamma_B/\Gamma_C)\exp(-K_B/We + K_C\sqrt{We})}{1 + (\Gamma_B/\Gamma_C)\exp(-K_B/We + K_C\sqrt{We})}, \quad (5)$$

where Γ_B, Γ_C, K_B, and K_C are constants. We is the Weber number defined by

$$We = \frac{\rho_f \varepsilon^{2/3} D_b^{5/3}}{\sigma}, \quad (6)$$

where ε and D_b are the energy dissipation rate per unit mass and the bubble diameter, respectively. The energy dissipation rate per unit mass is simply calculated from the mechanical energy equation as [20]

$$\varepsilon = \frac{\langle j\rangle}{\rho_m}\left(-\frac{dP}{dz}\right)_F, \quad (7)$$

where j, ρ_m and $(-dP/dz)_F$ are the mixture volumetric flux, the mixture density, and the gradient of the frictional pressure loss along the flow direction, respectively. The two-phase frictional pressure loss can be estimated by Lockhart–Martinelli's method [21]. For example, the gradient of the frictional pressure loss along the flow direction in turbulent flows for gas and liquid phases is given by

$$\left(-\frac{dP}{dz}\right)_F = \frac{0.158\rho_f v_f^{0.25}\Phi_f^2\langle j_f\rangle^{1.75}}{D^{1.25}}, \quad (8)$$

where v_f is the kinematic viscosity and Φ_f^2 is the two-phase frictional multiplier based on pressure gradient of liquid flow, which is a function of physical properties in the case of turbulent flows for gas and liquid phases. Substituting Eqs. (7) and (8) into Eq. (6) yields

$$We = 0.292\left(\frac{\rho_f^{1.67} v_f^{0.167}}{\sigma\rho_m^{0.667}}\right)\left(\frac{D_b^{1.67}\Phi_f^{1.33}\langle j_f\rangle^{0.667}\langle j\rangle^{0.833}}{D^{0.833}}\right), \quad (9)$$

Eq. (5) suggests that the bubble coalescence is more pronounced for smaller Weber number at a constant void fraction. In other words, the void fraction at the transition from bubble coalescence dominant flow to bubble breakup dominant flow is lowered by decreasing the Weber number. As can be seen from Eq. (9), since the Weber number is inversely proportional to the pipe diameter to the 0.833 power, the void fraction at the transition is lowered by increasing the pipe diameter and the bubble coalescence is more pronounced for a larger pipe at the same flow condition. Thus, it can be considered that a large diameter pipe tends to form cap bubbles easily.

3.1.3. Bubble Sauter mean diameter

Fig. 6 shows bubble Sauter mean diameter profiles of downward bubbly flows measured in vertical pipes with $D = 25.4$ mm (upper figure) and 50.8 mm (lower figure). The meanings of the symbols in Fig. 6 are found in Table 1. The bubble Sauter mean diameter profiles are almost uniform along the channel radius when no cap bubble is formed ($D = 25.4$ mm: ●, ▲ for $\langle j_f\rangle = -1.25$ m/s, ● for $\langle j_f\rangle = -2.12$ m/s, ●, ▲ for $\langle j_f\rangle = -3.11$ m/s; $D = 50.8$ mm: ●, ▲ for $\langle j_f\rangle = -0.620$ m/s, ● for $\langle j_f\rangle = -1.25$ m/s, ● for $\langle j_f\rangle = -2.49$ m/s). For $D = 25.4$ mm, as cap bubbles are formed (■ for $\langle j_f\rangle = -1.25$ m/s, ▲ for $\langle j_f\rangle = -2.12$ m/s), the bubble Sauter mean diameter profiles come to have a broad peak around the channel center. On the other hand, for $D = 50.8$ mm, as cap bubbles are formed (▲, ■ for $\langle j_f\rangle = -1.25$ m/s, ▲, ■ for $\langle j_f\rangle = -2.49$ m/s), the bubble Sauter mean diameter profiles come to be almost uniform along the channel radius with some increase in size near the wall.

The bubble Sauter mean diameter profile depending on the pipe diameter may be explained as follows. For example, the cap bubble diameters in the conditions such as $\langle\alpha\rangle = 15.5\%$, $\langle j_f\rangle = -2.12$ m/s and $D = 25.4$ mm, and $\langle\alpha\rangle = 5.20\%$, $\langle j_f\rangle = -2.49$ m/s and $D = 50.8$ mm are measured to be around 20 mm. Since the cap bubble diameter is comparable to the pipe size of $D = 25.4$ mm, lateral motion of the cap bubbles in the 25.4 mm-diameter pipe is limited by the presence of the pipe wall resulting in the core-peaked bubble diameter profile. On the other hand, the cap bubbles formed in the 50.8 mm-diameter pipe can be moved laterally, and in fact Fig. 2 shows that the cap bubbles stay near the channel wall resulting in the uniform bubble diameter profile with some increase near the wall.

3.1.4. Interfacial area concentration

Fig. 7 shows interfacial area concentration profiles of downward bubbly flows measured in vertical pipes with $D = 25.4$ mm (upper figure) and 50.8 mm (lower figure). The meanings of the symbols in Fig. 7 are found in Table 1. As expected for a bubbly flow, the interfacial area concentration profiles are similar to the void fraction profiles except for the flow conditions where cap bubbles appear. The interfacial area concentration is proportional to the void fraction and inversely proportional to the bubble Sauter mean diameter. Therefore, when the bubble Sauter mean diameter profiles are almost uniform along the channel radius, the interfacial area profiles display the same behavior as their respective void fraction profiles.

Since the formation of cap bubbles decreases the interfacial area concentration significantly, the interfacial area concentration profiles are different from the void fraction profiles for the flow condition where cap bubbles appear. For example, although the void fraction profile for $\langle\alpha\rangle = 5.20\%$, $\langle j_f\rangle = -2.49$ m/s and $D = 50.8$ mm (■) has an off-center peak, the interfacial area concentration profile comes to be almost uniform along the channel radius with a relatively sharp decrease near the wall.

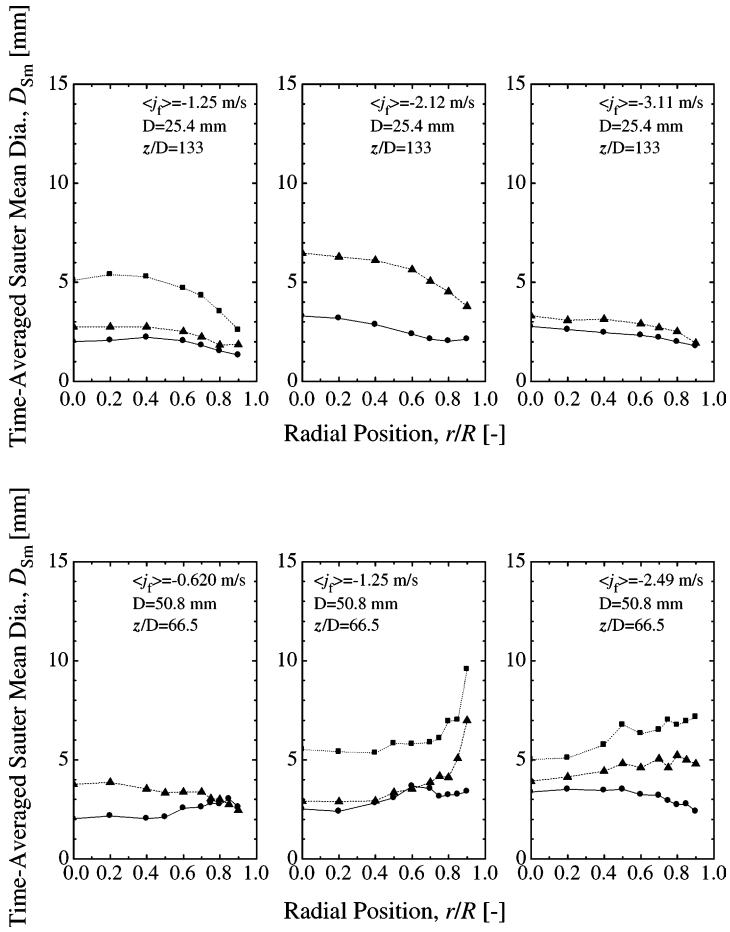

Fig. 6. Local bubble Sauter mean diameter profiles of downward bubbly flows measured in vertical pipes with $D = 25.4$ mm (upper figure) and 50.8 mm (lower figure).

3.1.5. Interfacial velocity

Fig. 8 shows interfacial velocity profiles of downward bubbly flows measured in vertical pipes with $D = 25.4$ mm (upper figure) and 50.8 mm (lower figure). The meanings of the symbols in Fig. 8 are found in Table 1. For most cases, the interfacial velocity profiles show the power-law profiles. As a general trend, for low liquid velocity, the introduction of bubbles into the liquid flow flattens the interfacial velocity profile, whereas the increase in liquid velocity diminishes the effect of the bubble on the interfacial velocity profile. The similar phenomena has also been reported in an upward flow [4,5]. However, for low liquid velocity such as $\langle j_f \rangle = -0.620$ m/s, the location of the maximum interfacial velocity occurs near the wall. This may be explained as follows.

Wang et al. [6] reported based on their measurements for $\langle j_f \rangle \leqslant 0.94$ m/s that in two-phase flows, the presence of voids tended to flatten the liquid velocity profile for both up and down flows. For the most down flows in their experiments, the location of the maximum liquid velocity occurred off the channel center and the bubble "coring" in down flows retarded the flow in the core due to buoyancy, and the resultant diversion of liquid into the low void region near the wall apparently caused the maximum liquid velocity to again occur near the wall. The similar observation was also reported by Kashinsky and Randin [8]. Since the interfacial velocity profile is expected to be similar to the liquid velocity profile, the peak in the velocity profile for the gas phase near the wall may be attributed to that for liquid phase.

3.2. One-dimensional flow parameters

3.2.1. Evaluation of drift-flux model for downward two-phase flow

In what follows, the drift-flux model for a downward two-phase flow developed by the authors based on existing area-averaged data [22] will be compared with the present experimental data [9] measured by the multi-

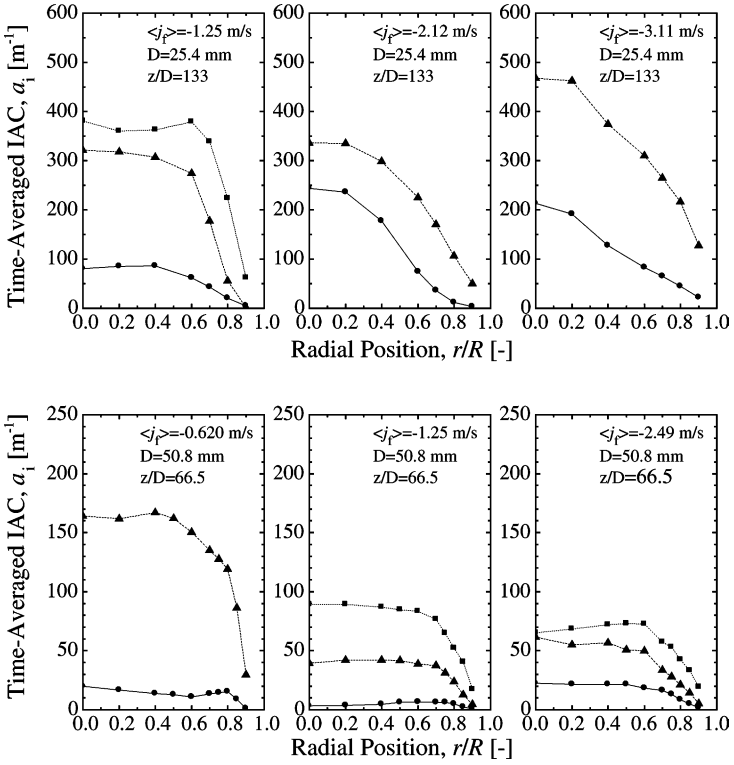

Fig. 7. Local interfacial area concentration profiles of downward bubbly flows measured in vertical pipes with $D = 25.4$ mm (upper figure) and 50.8 mm (lower figure).

sensor conductivity probe, and some discussions on the distribution parameter will be made based on assumed local void fraction profile. The non-dimensional form of the drift-flux model for a downward two-phase flow [22] is given as

$$\langle\langle v_g^* \rangle\rangle = C_0 \langle j^* \rangle + 1, \quad \text{where}$$
$$\langle\langle v_g^* \rangle\rangle = \langle\langle v_g \rangle\rangle / V_{gj} \text{ and } \langle j^* \rangle = \langle j \rangle / V_{gj}. \tag{10}$$

Here, $\langle\langle\ \rangle\rangle$ means the void-fraction weighted cross-sectional area-averaged quantity.

Since sufficient data of local flow parameters were not available, it was difficult to develop the detailed drift-flux model. Instead, Hibiki et al. [22] developed the approximated drift-flux model, which can be applicable to a wide flow range in downward flow. As the first assumption, Hibiki et al. [22] approximated the void-fraction weighted cross-sectional area-averaged drift velocity, V_{gj}, over all flow regimes to be Eq. (11), which is the same functional form as Ishii's Eq. [23] for the drift velocity of upward churn-turbulent flow.

$$V_{gj} = \sqrt{2}\left(\frac{g\sigma\Delta\rho}{\rho_f^2}\right)^{1/4}, \tag{11}$$

It should be noted here that the drift velocity for slug flow would be similar to that for bubbly and churn-turbulent flows for the data base utilized in the development of the drift-flux model. For example, for $D = 50.8$ mm, the drift velocity for slug flow calculated by Ishii's equation ($= 0.247$ m/s) is very close to that for churn-turbulent flow calculated by Eq. (11) ($= 0.231$ m/s). Even for $D = 16$ mm, the drift velocity for slug flow ($= 0.139$ m/s) is close to that for churn-turbulent flow ($= 0.231$ m/s). In addition, it was observed that the slug flows in downward flows were more chaotic, similar to the churn-turbulent flow in upward flows. For large diameter round tubes, slug bubbles cannot be formed due to the surface instability of slug bubbles. As far as the drift velocity for churn flow, Eq. (11), is not applied to estimate the drift velocity in capillary tubes, Hibiki et al. [22] concluded that Eq. (11) may give a good prediction for the drift velocity over all flow regimes. It should also be pointed out that the error in $\langle\langle v_g^* \rangle\rangle$ estimation due to the uncertainty of this assumption in the drift velocity would be less than $\pm 10\%$ for $\langle j^* \rangle \leqslant -5$ for conservative estimation.

Hibiki et al. [22] determined the distribution parameters by Eqs. (10) and (11) with measured void fraction, and superficial gas and liquid velocities, and then found that the distribution parameter might correlate closely with the non-dimensional mixture volumetric flux. The experimental result showed that the distribution

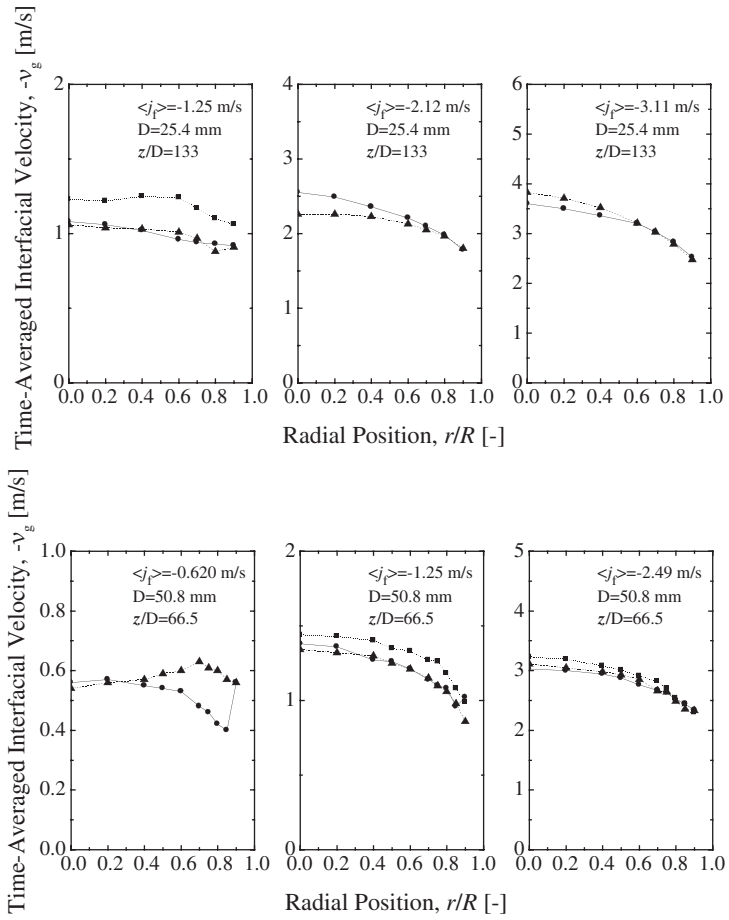

Fig. 8. Local interfacial velocity profiles of downward bubbly flows measured in vertical pipes with $D = 25.4$ mm (upper figure) and 50.8 mm (lower figure).

parameter increased up to a certain value and gradually decreased and eventually approached to unity as the downward mixture volumetric flux increased. This trend suggested the following function form for the distribution parameter in downward two-phase flow as:

$$C_0 = (-0.0214\langle j^* \rangle + 0.772) + (0.0214\langle j^* \rangle + 0.228)\sqrt{\frac{\rho_g}{\rho_f}} \quad \text{for } -20 \leqslant \langle j^* \rangle \leqslant 0,$$

$$C_0 = (0.2e^{0.00848(\langle j^* \rangle + 20)} + 1.0) - 0.2e^{0.00848(\langle j^* \rangle + 20)}\sqrt{\frac{\rho_g}{\rho_f}} \quad \text{for } \langle j^* \rangle < -20. \tag{12}$$

Here, the maximum value of the distribution parameter and the non-dimensional mixture volumetric flux at the maximum distribution parameter were experimentally determined to be 1.2 and −20, respectively, in order to obtain Eq. (12) [22]. In what follows, the validity of the assumed distribution parameter will be proven by a simple analysis with observed void fraction and interfacial velocity profiles.

The value of the distribution parameter can be estimated from assumed profiles of the void fraction and the mixture volumetric flux. By assuming a power-law profile in a pipe for the mixture volumetric flux, we have

$$\frac{j}{j_C} = 1 - \left(\frac{r}{R}\right)^m, \tag{13}$$

where the subscript of C means the value of the channel center and m is the exponent. Although three types void distributions such as off-center-peaked, bell-typed, and core-peaked distributions appear in a downward flow, the distribution parameter will take a maximum value for the bell-typed or core-peaked void distributions. To simulate the bell-typed distribution for the void fraction, we assume a power-law profile in a center region of a pipe for the void fraction, we have

$$\frac{\alpha}{\alpha_C} = 1 - \left(\frac{r}{R_P}\right)^n \quad \text{for } 0 \leqslant r \leqslant R_P,$$
$$\frac{\alpha}{\alpha_C} = 0 \quad \text{for } R_P \leqslant r \leqslant R, \tag{14}$$

where R_P and n are the radial position where the void fraction becomes zero and the exponent, respectively. It should be noted here that Eq. (14) can also simulate the core-peaked void distribution by setting R_P at unity.

By substituting these profiles into the definition of C_0, we obtain

$$C_0 = \frac{\langle \alpha j \rangle}{\langle \alpha \rangle \langle j \rangle} = \frac{1}{m}\left\{(m+2) - \frac{2(n+2)}{m+n+2}\left(\frac{R_P}{R}\right)^m\right\} = \frac{1}{m}\left\{(m+2) - \frac{2(n+2)}{m+n+2}x_B^m\right\}, \tag{15}$$

where x_B is a parameter defined by R_P/R. Fig. 9 shows the distribution parameters calculated by Eq. (15). The existing data of the void fraction profile [6–9] indicate that the minimum value of x_B is approximated to be 0.8 for a conservative estimate. The value of the distribution parameter for $x_B = 0.8$ is estimated to be about 1.25. Thus, the maximum value of the distribution parameter is less than 1.25 even for the bell-typed void fraction distribution. Thus, it can be concluded that the maximum value of the distribution parameter assumed in finalizing the drift-flux model would be a good approximation.

In addition to this, as shown in Figs. 2 and 8, the off-center-peaked distributions in void fraction and gas velocity found in relatively low liquid velocities tends to decrease the distribution parameter, resulting in the value less than unity. The mixture volumetric flux profile is more or less parabolic and thus the distribution parameter is insensitive to the exponent in Eq. (13) [24]. Particularly, for the off-center-peaked void distributions, the void fraction distribution may be a dominant factor to determine the distribution parameter [24]. Therefore, it can be recognized that the distribution parameter given by Eq. (12) approximately captures the true phase distribution.

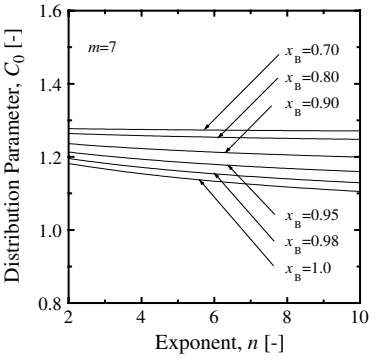

Fig. 9. Analytical prediction of distribution parameters.

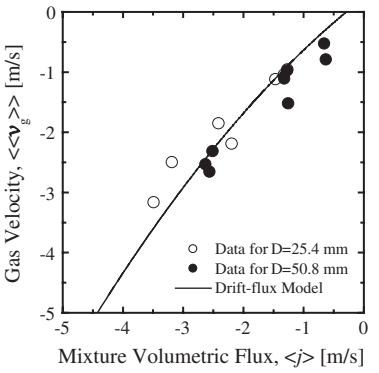

Fig. 10. Comparison of drift-flux model with downward flow data.

Fig. 10 shows the comparison of the drift-flux model with the data obtained by integrating local flow data measured by the authors [9] over the flow channel. The data agree with the drift-flux model within an average relative derivation of ±18.5%.

3.2.2. Evaluation of interfacial area concentration correlation

Recently, Hibiki and Ishii [25] developed the correlation of the interfacial area concentration for a steady fully developed bubbly flow from the interfacial area transport equation with extensive upward and horizontal flow data. In what follows, the applicability of the correlation to a downward bubbly flow will be examined by the present experimental data [9].

The correlation of the interfacial area concentration is given by

$$\tilde{a}_i = 3.02\widetilde{Lo}^{0.335}\alpha\widetilde{Re}^{0.239} \quad \text{or}$$
$$\tilde{D}_{Sm} = 1.99\widetilde{Lo}^{-0.335}\widetilde{Re}^{-0.239}, \tag{16}$$

where the non-dimensional interfacial area concentration, $\tilde{a}_i$, Laplace length scale, Lo, non-dimensional Laplace length scale, $\widetilde{Lo}$, and Reynolds number, $\widetilde{Re}$, are defined as follows:

$$\tilde{a}_i \equiv a_i Lo, \quad Lo \equiv \sqrt{\frac{\sigma}{g\Delta\rho}}, \quad \widetilde{Lo} \equiv \frac{Lo}{D_H}, \quad \text{and}$$
$$\widetilde{Re} \equiv \frac{(\varepsilon^{1/3}Lo^{1/3})Lo}{\nu_f}. \tag{17}$$

Here, D_H is the hydraulic equivalent diameter.

Fig. 11 compares measured interfacial area concentrations in downward bubbly flows with Eq. (16). As shown in Fig. 11, the correlation of the interfacial area concentration, Eq. (16), can approximately be applicable even to the downward bubbly flows with a relatively low

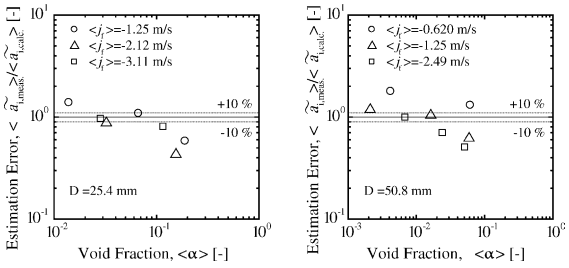

Fig. 11. Comparison of interfacial area correlation with downward flow data.

void fraction where no cap bubbles are formed. As cap bubbles are formed, Eq. (16) tends to overestimate the interfacial area concentrations in the downward bubbly flow.

4. Conclusions

In view of the great importance to two-fluid model, structure of a vertical downward bubbly flow has been discussed intensively based on available data sets of local flow parameters including extensive data sets recently measured by the authors. The important results obtained in this study are summarized as follows.

(1) An approximate phase distribution pattern map for a vertical downward two-phase flow has been proposed by available data sets. The phase distribution pattern in a downward two-phase flow can roughly be classified into three basic distributions, namely, (i) off-center-peaked, (ii) bell-typed, and (iii) core-peaked distributions. The mechanism determining the phase distribution pattern has been discussed based on lift force, wall repulsion force, and wall-vortex effect models. The phase distribution pattern map proposed in this study is expected to give a rough insight to understand the phase distribution pattern in a downward two-phase flow.
(2) Distribution patterns of local flow parameters such as interfacial area concentration, interfacial velocity, and bubble Sauter mean diameter have been shown and the mechanisms to determine the distribution patterns have been discussed.
(3) The one-dimensional drift-flux model for a vertical downward two-phase flow has been evaluated by the data sets measured by the present authors. The drift-flux model gives a fairly good prediction of the gas velocity in the downward two-phase flow.
(4) The correlation of the interfacial area concentration, which was developed based on extensive upward and horizontal flow data, has been evaluated by the data sets measured by the present authors. The interfacial area correlation gives a fairly good prediction of the interfacial area concentration in the downward two-phase flows with no cap bubbles. As cap bubbles are formed, the correlation tends to overestimate the interfacial area concentrations.

Acknowledgements

They would like to thank Prof. Tomoji Takamasa (Tokyo University of Marine Science and Technology, Japan) for his fruitful discussions. This work was supported by the USNRC Office of Nuclear Regulatory Research.

Appendix A

The conductivity probe method is capable of getting reliable local parameters of two-phase flow. However, due to the localization of the information, it would be impossible to instantaneously retrieve global information beyond where the sensor locates. This raises a problem on the categorization of bubbles according to local signal probe, if the chord length of the edge is less than the maximum distorted bubble length, then this signal will be considered a group-I bubble instead of the edge of a group-II bubble [26]. Therefore, the overall bubble number as well as the void fraction and interfacial area concentration of group-II bubbles will be underestimated as follows.

A counted bubble is classified into a group according to its chord length in the axial direction. For an air–water adiabatic flow at room temperature, the criteria used to distinguish spherical or distorted bubbles and cap or slug bubbles are below 10 mm and above 10 mm, respectively. Thus, a considerable off-center part of a group-II bubble may not be categorized as a group-II bubble, unless the bubble is far larger than the threshold bubble diameter.

If the chord length of a bubble is longer than the threshold value, $D_{d,max}$ the signal from the probe is categorized as that from a group-II bubble. The volume fraction of the center part of a group-II bubble categorized as a group-II bubble, ω, can be derived from a simple geometrical consideration under three assumptions that (i) a bubble shape is hemi-spherical; (ii) a probe passes every part of bubble with an equal probability and (iii) the minimum and maximum size of two-group bubbles are $D_{d,max}$ and $D_{b,2,max}$, respectively, and the bubble number density distribution function is constant between $D_{d,max}$ and $D_{b,2,max}$. The volume fraction, ω, can be calculated as the ratio of the volume of a part categorized as a group-II bubble by the chord length to the total volume of the bubble.

$$\omega = \frac{D_{b,2}^{*3} - 4}{D_{b,2}^{*3}}, \tag{A.1}$$

where $D_{b,2}^{*} \equiv \frac{D_{b,2}}{D_{d,max}}$ and $D_{b,2}$ is the size of the group-II bubble. If we assume a spherical bubble, the volume fraction, ω, can be expressed as

$$\omega = \frac{D_{b,2}^{*3} - 1}{D_{b,2}^{*3}}. \tag{A.2}$$

In Fig. 12, the volume fraction, ω, is plotted against the non-dimensional bubble diameter, $D_{b,2}^{*}$. For example, if the average bubble size is 3, about 85% of the total volume of group-II bubbles is categorized as the volume of the group-II bubbles. In the present experiment, $D_{b,2}^{*}$ is about 3 [9]. Thus, even though no correction for the approximate classification of the bubble group based on the chord length is made, the classification error may be estimated to be less than 15% in the present flow conditions for a conservative estimate. It should be noted here that such approximate classification does not cause extra measurement error in total void fraction and interfacial area concentration.

In the signal processing software used in the experiment, the correction scheme for the miss-counted bubble number as well as the void fraction and the interfacial area contributions has been developed [26]. Based on a scale analysis of the number of group-I and group-II bubbles, a simple correction scheme can be given by

$$\alpha_{1,A} = \alpha_{1,B} - \alpha_{1,B}\frac{N_2}{N_1 + N_2} \quad \text{and}$$
$$\alpha_{2,A} = \alpha_{2,B} + \alpha_{1,B}\frac{N_2}{N_1 + N_2}, \tag{A.3}$$

and

$$a_{i,1,A} = a_{i,1,B} - a_{i,1,B}\frac{N_2}{N_1 + N_2} \quad \text{and}$$
$$a_{i,2,A} = a_{i,2,B} + a_{i,1,B}\frac{N_2}{N_1 + N_2}, \tag{A.4}$$

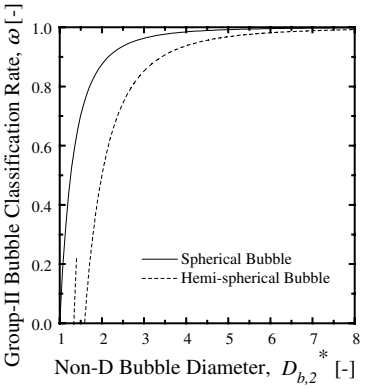

Fig. 12. Volume fraction of center part of a group-II bubble categorized as a group-II bubble.

where N_1 and N_2 are the bubble numbers of each group, and the subscripts A and B denote the quantities after and before the correction, respectively. When bubble number ratio $N_2/N_1 \ll 1$, this correction would give satisfactory results [26]. An option is set in the signal processing software for this correction scheme to be employed and the detailed explanation of this correction scheme is described somewhere [26].

References

[1] A. Serizawa, I. Kataoka, Phase distribution in two phase-flow, in: N.H. Afgan (Ed.), Transient Phenomena in Multiphase Flow, Hemisphere, Washington, DC, 1988, pp. 179–224.

[2] W.H. Leung, S.T. Revankar, Y. Ishii, M. Ishii, Axial development of interfacial area and void concentration profiles measured by double-sensor probe method, Int. J. Heat Mass Transfer 38 (1995) 445–453.

[3] C. Grossetete, Caracterisation experimentale et simulations de l'evolution d'un ecoulement diphasique a bulles ascendant dans une conduite verticale, Ph.D. Thesis, Ecole Centrale Paris, France, 1995.

[4] T. Hibiki, M. Ishii, Experimental study on interfacial area transport in bubbly two-phase flows, Int. J. Heat Mass Transfer 42 (1999) 3019–3035.

[5] T. Hibiki, M. Ishii, Z. Xiao, Axial interfacial area transport of vertical bubbly flows, Int. J. Heat Mass Transfer 44 (2001) 1869–1888.

[6] S.K. Wang, S.J. Lee, O.C. Jones Jr., R.T. Lahey Jr., 3-D turbulence structure and phase distribution measurements in bubbly two-phase flows, Int. J. Heat Mass Transfer 13 (1987) 327–343.

[7] K. Usui, K. Sato, Vertically downward two-phase flow, (I) Void distribution and average void fraction, J. Nuclear Sci. Technol. 26 (1989) 670–680.

[8] O.N. Kashinsky, V.V. Randin, Downward bubbly gas–liquid flow in a vertical pipe, Int. J. Multiphase Flow 25 (1999) 109–138.

[9] M. Ishii, S. Kim, H. Goda, S.S. Paranjape, J. Finch, Interpretation of results for interfacial area measurements (2.54-cm and 5.08-cm downward flow data and analysis), Purdue University Technical Report, PU NE-01-05, School of Nuclear Engineering, Purdue University, West Lafayette, IN, USA, 2001.

[10] S. Kim, X.Y. Fu, X. Wang, M. Ishii, Development of the miniaturized four-sensor conductivity probe and the signal processing scheme, Int. J. Heat Mass Transfer 43 (2000) 4101–4118.

[11] T. Hibiki, R. Situ, Y. Mi, M. Ishii, Local flow measurements of vertical upward bubbly flow in an annulus, Int. J. Heat Mass Transfer 46 (2003) 1479–1496.

[12] T. Oshinowo, M.E. Charles, Vertical two-phase flow, Part I. Flow pattern correlations, Canad. J. Chem. Eng. 52 (1974) 25–35.

[13] B.G. Ganchev, V.G. Peresadko, Hydrodynamic and heat transfer processes in descending bubble flows, J. Eng. Phys. 49 (1985) 181–189.

[14] I. Zun, Transition from wall void peaking to core void peaking in turbulent bubbly flow, in: N.H. Afgan (Ed.),

Transient Phenomena in Multiphase Flow, Hemisphere, Washington, DC, 1988, pp. 225–245.
[15] A. Tomiyama, H. Tamai, I. Zun, S. Hosokawa, Transverse migration of single bubbles in simple shear flows, Chem. Eng. Sci. 57 (2002) 1849–1858.
[16] S.P. Antal, R.T. Lahey Jr., J.E. Flaherty, Analysis of phase distribution in fully developed laminar bubbly two-phase flow, Int. J. Multiphase Flow 17 (1991) 635–652.
[17] Z. Rohani, Effect of wall friction and vortex generation on radial void distribution—the wall vortex effect, Aktiebolaget Atomenergi, Sweden, AE-497, 1974.
[18] M. Ishii, N. Zuber, Drag coefficient and relative velocity in bubbly, droplet or particulate flows, AIChE J. 25 (1979) 843–855.
[19] T. Hibiki, M. Ishii, Development of one-group interfacial area transport equation in bubbly flow systems, Int. J. Heat Mass Transfer 45 (2002) 2351–2372, The erratum has been published in 45 (2002) 3679–3680.
[20] G. Kocamustafaogullari, W.D. Huang, J. Razi, Measurement of modeling of average void fraction bubble size and interfacial area, Nucl. Eng. Design 148 (1994) 437–453.
[21] R.W. Lockhart, R.C. Martinelli, Proposed correlation of data for isothermal two-phase, two-component flow in pipes, Chem. Eng. Prog. 5 (1949) 39–48.
[22] T. Hibiki, H. Goda, S. Kim, M. Ishii, J. Uhle, One-dimensional drift-flux model for downward two-phase flow, in: Proceedings of 11th International Conference on Nuclear Engineering, Tokyo, Japan, April 20–23, 2003, Paper No. ICONE11-36015.
[23] M. Ishii, One-dimensional drift-flux model and constitutive equations for relative motion between phases in various two-phase flow regimes, ANL-77-47, USA, 1977.
[24] T. Hibiki, M. Ishii, Distribution parameter and drift velocity of drift-flux model in bubbly flow, Int. J. Heat Mass Transfer 45 (2002) 707–721.
[25] T. Hibiki, M. Ishii, Interfacial area concentration of bubbly flow systems, Chem. Eng. Sci. 57 (2002) 3967–3977.
[26] X. Fu, Interfacial area measurement and transport modeling in air–water two-phase flow, Ph.D. Thesis, School of Nuclear Engineering, Purdue University, West Lafayette, IN, USA, 2001.